

Rejection-based sampling of inelastic neutron scattering

X.-X. Cai^{a,b,*}, T. Kittelmann^b, E. Klinkby^{a,b}, J.I. Márquez Damián^c

^a*Technical University of Denmark, Denmark*

^b*European Spallation Source ERIC, Sweden*

^c*Nuclear Data Group, Neutron Physics Department, Centro Atómico Bariloche, CNEA, Argentina*

Abstract

Distributions of inelastically scattered neutrons can be quantum dynamically described by a scattering kernel. We present an accurate and computationally efficient rejection method for sampling a given scattering kernel of any isotropic material. The proposed method produces continuous neutron energy and angular distributions, typically using just a single interpolation per sampling. We benchmark the results of this method against those from accurate analytical models and one of the major neutron transport codes. We also show the results of applying this method to the conventional discrete double differential cross sections.

1. Introduction

The neutron scattering kernel [1], also known as the scattering law or the scattering function, is defined by the dynamical properties of a material and the associated scattering lengths of the probing neutron, and is a function of energy- and momentum-transfers. Described by a scattering kernel, the vibrational excitations and atomic diffusive motions are fingerprinted in the double differential scattering cross sections. Concerning neutron scattering in condensed matter, scattering kinematics are often simulated by Monte Carlo methods to relate measurements to underlying physics. When the distributions related to individual scatterings are important, such as when performing data correction or characterisation at neutron scattering instruments [2], the scattering

*Corresponding author:
Email address: xcai@dtu.dk (X.-X. Cai)

is sampled directly from the scattering kernel in order to reproduce the measured double differential cross sections. The energy region of interest in such applications is typically below 100 milli-electronvolt. On the other hand, in neutronics applications, e.g. [3], scattered neutron states are traditionally sampled from the pre-processed double differential cross sections in either continuous or discrete forms for incident neutrons up to a few electronvolt. However, in recent years, attracted by its small memory footprint and the absence of geometrical limits to its validity, the method of directly sampling from scattering kernels [4] has been implemented in a few neutronic codes as well [5, 6, 7].

The concept of rejection-based Monte Carlo sampling is well suited for neutron scattering, as the analytical expression required for sampling via the transformation method generally does not exist. However, if the bounding distribution is not chosen with care, the computational efficiency of this method may be unacceptable. For example, a prior attempt of sampling 1eV neutron scattering with hydrogen in water showed less than 0.1% acceptance rate [5].

The scope of this paper is to present an accurate and efficient method for sampling a given scattering kernel. Section 2 introduces our method to sample the kernels for isotropic materials. For the purpose of verifying the rejection method presented here, we compare its predictions with results from analytical models and one of the major Monte Carlo neutron transport codes in section 3. Methods of applying this rejection method to the commonly used discrete cross sections is also discussed in this section. We conclude this work in section 4.

2. Method

Given a scattering kernel S , for a material at temperature T , the relationship between bound and double-differential cross section per atom is given by [4]¹

$$\frac{\partial^2 \sigma}{\partial E' \partial \Omega} = \frac{\sigma_b k'}{4\pi k} S(Q, \omega) = \frac{\sigma_b}{4\pi} \sqrt{\frac{E'}{E}} \frac{S(\alpha, \beta)}{k_b T} \quad (1)$$

¹For simplicity, S used in this work is assumed to be an asymmetric scattering function, but it would be straight-forward to apply the presented sampling method to symmetric scattering kernels.

with

$$\alpha = \frac{E + E' - 2\mu\sqrt{E'E}}{k_b T} \quad \text{and} \quad \beta = \frac{E' - E}{k_b T} \quad (2)$$

Here α is the momentum transfer, β is the energy transfer, σ and σ_b are the scattering and bound cross sections, respectively, μ is the cosine of the scattered angle, k_b is the Boltzmann constant, T is the temperature, E and E' are the incident and scattered energies, respectively, and k and k' are the wavevectors before and after the scattering. Notice that the definition of α here differs from that in NJOY [3], which mainly concerns incoherent scattering kernels, by the factor M/m , where M and m are the target and neutron masses, respectively. Inclusion of target masses in the formulas is not problematic for incoherent scattering, where separate contributions from scattering on atoms with different masses is additive. But in a coherent kernel, scattering originates from correlations of different atoms, and the definition of a target mass is thus ambiguous for any material which does not consist of a single isotope. In either case, however, to represent a valid scattering, α and β should satisfy two conditions: firstly, the scattered energy must be non-negative, thus the value of β should not be less than $\beta_- = -E/kT$. ; secondly, the cosine of the scattered angle must be in $[-1, 1]$. Accordingly, the lower and upper bounds on α can be expressed as a function of energy transfer [4].

$$\alpha_{\pm}(\beta) = \frac{2E + k_b T \beta \pm 2\sqrt{E(E + k_b T \beta)}}{k_b T} \quad (3)$$

The integral scattering cross section can be evaluated as [4]

$$\sigma(E) = \frac{C}{E} \int_{-\infty}^{\infty} \int_{-\infty}^{\infty} S(\alpha, \beta) \Theta(\alpha, \beta) d\alpha d\beta \quad (4)$$

where C is a constant that equals $\sigma_b k_b T / 4$, and

$$\Theta(\alpha, \beta) = \begin{cases} 1 & \text{when } (\alpha, \beta) \in D \\ 0 & \text{otherwise} \end{cases} \quad (5)$$

Here the region D represents the entire valid scattering phase-space of incident neutrons at E , and can be expressed as

$$D = \{(\alpha, \beta) : \beta \geq -E/k_b T \quad \text{and} \quad \alpha_-(\beta) \leq \alpha \leq \alpha_+(\beta) \} \quad (6)$$

It can be shown that the signs of the first derivative of α_- and α_+ are non-positive and positive, respectively, for any incident energy, while β_- obviously decreases with increasing incident energy. In other words, D is a monotonically expanding region with increasing incident energy.

In terms of sampling, it can be seen from Eq. 4 that the conditional probability density function (PDF) is

$$p(\alpha, \beta | E) = \frac{C}{\sigma(E)E} S(\alpha, \beta) \Theta(\alpha, \beta) \quad (7)$$

It is relatively computational intensive to construct such a distribution in either continuous or discrete forms, thus on-the-fly determination of p is often avoided in Monte Carlo simulations. Numerically, this distribution has instead been approximated by interpolating the sampled results, from the distribution of a slightly higher energy neutron and that of a slightly lower energy neutron, with respect to the actual incident energy. As a better alternative, we here propose a sampling method that can skip this approximation, thus eliminating potential errors associated with the interpolations. To do so, it is desired to develop the PDF further into the form of $p(x) = A^{-1} p_1(x) h(x)$, where A^{-1} is a normalisation factor, p is a PDF of x on a two dimensional space, and h is a scalar function in the range between 0 and 1. Suggested by item R13 in [8], a PDF in this form can be sampled by the rejection-based Monte Carlo method. Briefly, the first step is to sample a value x from p_1 , along with a random number ξ drawn uniformly from $[0, 1]$, then either accept x if $\xi \leq h(x)$, or sample a new value of x and repeat the procedure. The efficiency of this, i.e. the acceptance rate, is A .

Let E_l and E_h be the kinetic energies of two neutrons that satisfy $E_l < E_h$. Assuming the distribution for E_h is given, and only the scattered status of a neutron at E_l is of interest. From Eq. 7, we have

$$\frac{p(\alpha, \beta | E_l)}{p(\alpha, \beta | E_h)} = \frac{\sigma(E_h)E_h S(\alpha, \beta) \Theta_l(\alpha, \beta)}{\sigma(E_l)E_l S(\alpha, \beta) \Theta_h(\alpha, \beta)} \quad (8)$$

Notice that Eq. 8 is only well-defined within the region D_h . However, because of the energy-dependent expansion behaviour of D , D_h already covers the full region of interest, i.e. D_l , within which valid samples are all situated. In the region D_h , Θ_h

becomes unity, we can obtain

$$p(\alpha, \beta | E_l) = \frac{\sigma(E_h)E_h}{\sigma(E_l)E_l} p(\alpha, \beta | E_h) \Theta_l(\alpha, \beta) \quad (9)$$

To sample from Eq. 9, we first sample a pair of (α, β) at E_h , i.e. $p(\alpha, \beta | E_h)$, and then consider the acceptance of this sample according to Θ_l . Unlike the h function in the general case, its equivalent function, Θ , in this case equals either 0 or 1. Therefore, the generation of the random number ξ can be skipped. The acceptance rate in the case of Eq. 9 is

$$\mathcal{M}(E_l, E_h) = \sigma(E_l)E_l / \sigma(E_h)E_h \quad (10)$$

For a special case, in the so-called $1/v$ region, where the cross section is inversely proportional to the neutron incident speed, \mathcal{M} is simply $\sqrt{E_l/E_h}$. When a dense energy grid in the evaluated data library is used, \mathcal{M} is generally greater than 90% in the thermal neutron range.

In the rejection method, it is clear that the probability of accepting a sample for a neutron at a certain energy is \mathcal{M} . In terms of computational speed, the cost on the samples that are eventually dropped can be less than that, as sampling algorithms can be optimised by rejecting unsatisfied samples at an early stage, before the expensive part of the sampling algorithm. By default, all simulated data in the later sections of this paper are generated using Algorithm 1. However, a shortcoming of Algorithm 1 is that the timing behaviour is less straight forward to predict. As the worst case scenario for speed, the Algorithm 2, where the computational speed is proportional with the acceptance rate, is also implemented to help verifying the timing behaviour of the rejection method.

Algorithm 1: optimised for speed

- 1 find smallest i , so that
 $E \leq E_i$
- 2 **repeat**
- 3 | sample a β' from
 | $P(\beta | E_i)$
- 4 **until** $-E/k_b T \leq \beta$;
- 5 find j , so that $\beta_{j-1} \leq \beta' \leq \beta_j$
- 6 sample α_l from
 $F(\alpha | \beta_{j-1}, E_i)$
- 7 sample α_h from $F(\alpha | \beta_j, E_i)$
- 8 interpolate an α' from α_l and
 α_h
- 9 **if** $\alpha' \notin (\alpha_-, \alpha_+)$ **then** go to
 2 ;
- 10 **else** accept α' and β' ;

Algorithm 2: predictable speed

- 1 find smallest i , so that
 $E \leq E_i$
- 2 sample a β' from $P(\beta | E_i)$
- 3 find j , so that $\beta_{j-1} \leq \beta' \leq \beta_j$
- 4 sample α_l from
 $F(\alpha | \beta_{j-1}, E_i)$
- 5 sample α_h from $F(\alpha | \beta_j, E_i)$
- 6 interpolate an α' from α_l and
 α_h
- 7 **if** $\alpha' \notin (\alpha_-, \alpha_+)$, $\frac{-E}{k_b T} \leq \beta$
 then go to 2 ;
- 8 **else** accept α' and β' ;

2.1. Numerical approximations employed in the implementation

To evaluate the double integral in Eq. 4, we make a few approximations, which are independent from the proposed sampling method. To be compatible with the ENDF standard, it is assumed that $S(\alpha | \beta)$ can be interpolated by the log-linear law [3, 9], using which gives the following evaluation for the alpha integral over an interval $[\alpha_1, \alpha_2]$

$$\int_{\alpha_1}^{\alpha_2} S(\alpha | \beta) d\alpha = \frac{(\alpha_2 - \alpha_1)[S(\alpha_2 | \beta) - S(\alpha_1 | \beta)]}{\log[S(\alpha_2 | \beta)/S(\alpha_1 | \beta)]} \quad (11)$$

Applying the transformation method [8], it can be shown that an α value can be sampled as

$$\alpha = -xy^{-1} \log \left[\frac{S(\alpha_a | \beta) \exp(-\alpha_a y/x)}{r[(S(\alpha_b | \beta) - S(\alpha_a | \beta)) + S(\alpha_a | \beta)]} \right] \quad \text{with} \quad x = \alpha_b - \alpha_a \quad \text{and} \quad y = \log \left[\frac{S(\alpha_b | \beta)}{S(\alpha_a | \beta)} \right] \quad (12)$$

where $r = \xi_1 - \int_{\alpha_-}^{\alpha_a} S(\alpha|\beta) d\alpha / \int_{\alpha_-}^{\alpha_+} S(\alpha_a|\beta) d\alpha$ with $\xi_1 \in [0,1)$. In the implementations of both Algorithm 1 and 2, y is pre-computed and cached in memory for the entire (α, β) grid. To save memory, the actual implementation of the α distribution storage follows the method suggested in [4], in which the cumulative conditional distribution is converted into $F(\alpha_x|\beta) = \int_0^{\alpha_x} S(\alpha|\beta) d\alpha$ to decouple with incident energy.

For the outer beta integral of Eq. 4, a simple trapezoidal approximation is used over all β intervals

$$\sigma = \int_{\beta_2}^{\beta_1} F(\beta|E) d\beta \approx \frac{1}{2}(\beta_2 - \beta_1)[F(\beta_1|E) + F(\beta_2|E)] \quad (13)$$

It can be seen from Eq. 13 that $F(\beta|E)$ is proportional with the probability density of β , so it in fact can be used to generate point-wise linear functions, which are useful for sampling β . However, this low order trapezoidal approximation is often a major, if not the dominant, error source when approximating fine structures of energy transfer distributions, e.g. the quasi-elastic peak [10] in liquids that represents the diffusive motions. To minimize the numerical errors, the β grid used in caching is finer than the input kernel in some critical regions. We refer to this numerical procedure as the thickening process.

3. Benchmark and verification

3.1. Benchmarking the accuracy of implementation

For the purpose of benchmarking our implementation, we study the scattering in a classical monoisotopic ideal gas, where the scattering kernel, the total cross section and the scattered energy distribution can be expressed analytically at closed-form expression.

The gas system of interest consists of motion independent nuclei in an ensemble at 293.6K. Each nuclei moves freely with the speed distribution of a Maxwellian. The scattering kernel can be expressed analytically [11]. In dimensionless form [3], it can be expressed as.

$$S(\alpha, \beta) = \frac{\exp(-\beta/2)}{\sqrt{4\pi\alpha/A}} \exp\left[-\frac{\alpha^2/A^2 + \beta^2}{4\alpha/A}\right] \quad (14)$$

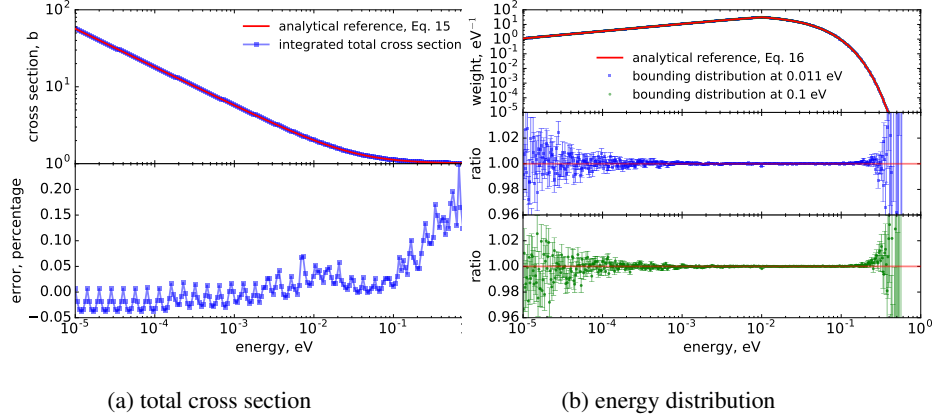


Figure 1 Neutron scattering with the hypothetical ideal gas in three different setups. Fig. 1a compares our implemented Eq. 4 and the analytical reference Eq. 15. Fig. 1b shows the scattered energy distributions of ten billion neutrons at 0.01 eV using the bounding distributions constructed at two higher energies. Error bars represent the root-mean-squared error. Results are benchmarked against the analytical reference Eq. 16.

where A is the ratio between the nucleus mass and the neutron mass.

For simplicity, if we assume the atomic mass is identical to the neutron mass, and the free scattering cross section is unity, the expressions of the total cross sections and energy differential cross section are particularly simple [12]. They are shown in Eq. 15 and 16.

$$\sigma(E) = \left(1 + \frac{1}{2a^2}\right) \operatorname{erf}(a) + \exp(-a^2)/(a\sqrt{\pi}) \quad \text{with} \quad a = \sqrt{E/k_bT} \quad (15)$$

$$f(E \rightarrow E') = \begin{cases} \exp(\beta) \operatorname{erf}(\sqrt{E'/kt})/[E\sigma(E)] & , E < E' \\ \operatorname{erf}(\sqrt{E'/kt})/[E\sigma(E)] & , E > E' \end{cases} \quad (16)$$

We simulate this hypothetical ideal gas and compare the results with these equations. The alpha and beta grids of the kernel used in the simulations are the same as those in the ENDF/B-VIII.0 H(H₂O) TSL evaluation [13], except for the density of the beta grid which is refined by a factor of two. The total cross section calculated by our implementation are compared with the analytical reference in Fig. 1a. The absolute error of our implementation is smaller than 0.05% below about 0.1 eV, trending towards 0.2% at 1 eV. Fig. 1b benchmarks the scattered energy distribution of 0.01 eV

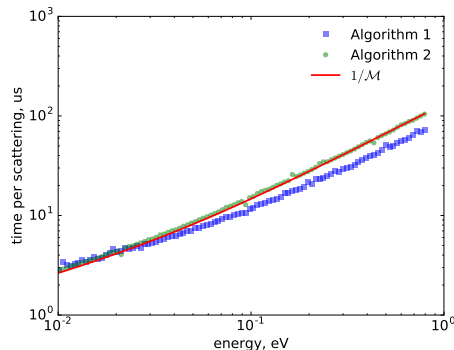


Figure 2 This figure shows the average speed to generate one success final state of a 0.01 eV neutron as a function of the energy where the bounding distributions created. the red curve is normalized to have the same area as the points of the Algorithm 1.

incident neutrons based on PDFs constructed at 0.011 eV and 0.1 eV. It can be observed that both the energy distributions are statistically equivalent to the analytical reference curve. The results from our implementation are in excellent agreement with the analytical references.

Shown in Fig. 2, the speed behaviour of Algorithm 1 is well described by $1/M$. Algorithm 2 shows noticeable speedup when the energy of the bounding distribution is considerably higher than the incident energy. The speedup grows with incident energy and up to about 45% when the bounding distribution is constructed at 0.8 eV.

3.2. Simulation of a water sphere in the free-gas approximation

We categorise the physics models based on scattering kernels or their derived data as *quantum models*, and the models that sample the scattering as elastic scattering with a thermally-excited nucleus in the centre-of-mass frame as *classical models*. When simulating a classical ideal gas system, these two types of models should in principle yield statistically equivalent results, apart from the numerical uncertainties due to the sampling procedure.

To test our numerical implementation, we simulate the volume flux of a free-gas approximated water sphere [14]. The water sphere has a radius of 30 cm, consists of $^1\text{H}_2^{16}\text{O}$, and with a density of 1 g/cm^3 . Neutron scattering with both hydrogen and oxygen are simulated by the kernel driven rejection method introduced in section 2.

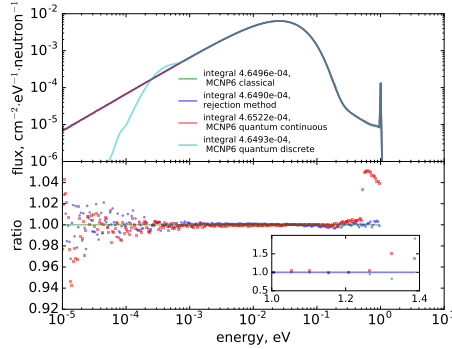
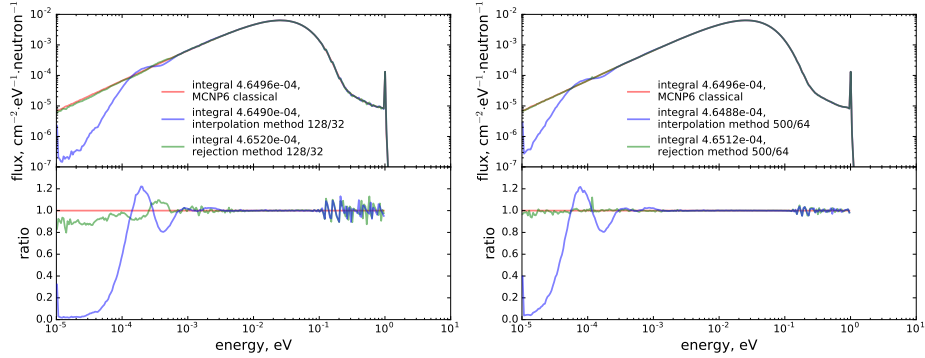


Figure 3 Free-gas treatment of the water sphere. The ratio between the MCNP6 quantum discrete and classical models is not shown.

The kernel for hydrogen is computed using the free gas model of the LEAPR model in NJOY. In the simulation, 100 million 1 eV neutrons are initialized with an isotropically distributed random direction at the centre of the sphere. We simulate scattering and capture processes. A neutron is removed from the simulation if it is captured, before reaching the surface of the sphere.

We compare our result with the results predicted by MCNP6 [15], in which thermal neutron scattering with hydrogen can be simulated classically, or by two alternative quantum models based on continuous and discrete double differential cross sections, respectively, whereas scattering with oxygen is always modelled using the classical model. NJOY is used to generate the continuous and discrete cross section files based on [13]. The energy grid contains 116 points in the range between 10^{-5} and 10 eV.

The results are shown Fig. 3. The result from the MCNP6 classical model is used as the reference. Between 10^{-3} eV and 1 eV, the fluxes predicted by the rejection method differ only a small fraction of percent from those predicted by the MCNP6 classical model. The fluctuations at the low energy end of the rejection method spectrum are due to statistical uncertainties, of which the extent is consistent with that in the spectrum of the MCNP6 continuous model in the same energy region. However, between 0.5 eV and the incident energy, i.e. 1 eV, the MCNP6 continuous model overestimated the fluxes by approximately 5%. A later work is performed to use the same continuous cross section with OpenMC [16] to try to identify the source of this overestimation.



(a) coarse grid ACE file, 128 energy and 32 angular bins

(b) fine grid ACE file, 500 energy and 64 angular bins

Figure 4 Water volume spectra simulation in the free-gas treatment using the discrete double differential cross sections. Spectra are compared with that the reference classical model.

Such overestimation can not be observed from the spectrum given by OpenMC, indicating that this artefact is originated from the sampling method implemented in MCNP6. Observed in Fig. 3, the quantum discrete model in general predicts a realistic integral flux but shows the same artefacts already observed in MCNP [14] below about 1 meV.

The rejection method can be directly applied to discrete cross section in ACE format. Fig. 4 compares the spectra given by the rejection method and the conventional interpolation method, of which neutron final state is interpolated from the distributions of adjacent energies. At the high energy ends, the fluctuations depend highly on the density of the energy and angular grid; while at the low energy ends, the errors are very sensitive to the sampling method chosen.

3.3. Simulation of a water sphere using a bound hydrogen kernel

Replacing the free-gas kernel of hydrogen by one including more realistic binding effects [10], we simulate the sphere again. The resulting volume spectra of our implementation and the MCNP6 quantum continuous model are compared in Fig. 5. At the high energy end, MCNP6 result shows a similar overestimation as in the free-gas case. At the low energy end, the spectrum from MCNP6 shows structures with fluctuations up to 65%, corresponding to about 3% of one standard deviation in that region.

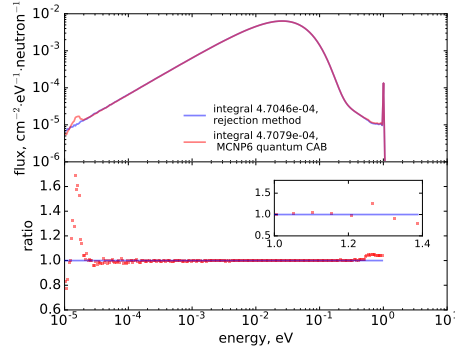


Figure 5 Bound hydrogen treatment of the water sphere. A realistic CAB scattering kernel for hydrogen [10] is used.

As the total cross sections in water below 10^{-4} eV should be featureless, satisfying the $\sigma \propto 1/v$ relation, such fluctuations are unphysical.

4. Conclusion

The proposed rejection method decouples the dependence on distributions of any lower energy neutrons, therefore requires fewer interpolations. It is accurate and overcomes some artefacts introduced by conventional interpolation methods. It is also straightforward for an existing code to adapt. Our implementation in this paper will be integrated into the software package NCrystal [17] in the upcoming releases.

Acknowledgements

This work was supported in part by the European Unions Horizon 2020 research and innovation programme under grant agreement No. 676548 (the BrightnESS project) and under grant agreement No. 654000 (the SINE2020 project).

References

- [1] L. Van Hove, “Correlations in space and time and Born approximation scattering in systems of interacting particles,” *Phys. Rev.*, vol. 95, no. 1, pp. 249–262, 1954.

- [2] E. Farhi, V. Hugouvieux, M. R. Johnson, and W. Kob, “Virtual experiments: Combining realistic neutron scattering instrument and sample simulations,” *Journal of Computational Physics*, vol. 228, no. 14, pp. 5251–5261, 2009.
- [3] R. MacFarlane and A. Kahler, “Methods for Processing ENDF/B-VII with NJOY,” *Nuclear Data Sheets*, vol. 111, pp. 2739–2890, dec 2010.
- [4] F. G. Bischoff and M. L. Yeater, “Monte Carlo evaluation of multiple scattering and resolution effects in double-differential neutron scattering cross-section measurements,” *Nucl. Sci. Eng.*, vol. 48, pp. 266–280, 1972.
- [5] C. T. Ballinger, “The direct $S(\alpha, \beta)$ method for thermal neutron scattering,” in *International Conference on Mathematics, Computational Methods, and Reactor Physics*, pp. 134–143, 1999.
- [6] A. T. Pavlou and W. Ji, “On-the-fly sampling of temperature-dependent thermal neutron scattering data for Monte Carlo simulations,” *Annals of Nuclear Energy*, vol. 71, pp. 411–426, sep 2014.
- [7] S. W. Hart and G. I. Maldonado, “Implementation of the direct $S(\alpha, \beta)$ method in the KENO Monte Carlo code,” *Annals of Nuclear Energy*, vol. 101, pp. 270–277, 2017.
- [8] C. J. Everett and E. D. Cashwell, “A Third Monte Carlo Sampler,” 1983.
- [9] A. Trkov, M. Herman, D. Brown, *et al.*, “ENDF-6 formats manual,” *Data Formats and Procedures for the Evaluated Nuclear Data Files ENDF/B-VI and ENDF/B-VII*, National Nuclear Data Center Brookhaven National Laboratory, Upton, NY, pp. 11973–5000, 2012.
- [10] J. Márquez Damián, J. Granada, and D. Malaspina, “CAB models for water: A new evaluation of the thermal neutron scattering laws for light and heavy water in ENDF-6 format,” *Annals of Nuclear Energy*, vol. 65, pp. 280–289, mar 2014.
- [11] G. L. Squires, *Introduction to the Theory of Thermal Neutron Scattering*, ch. 4.5. Cambridge, 1997.

- [12] W. M. Stacey, *Nuclear Reactor Physics*, ch. 12.2. Wiley-VCH, second ed.
- [13] D. A. Brown, M. B. Chadwick, R. Capote, A. C. Kahler, A. Trkov, M. W. Herman, A. A. Sonzogni, Y. Danon, A. D. Carlson, M. Dunn, D. L. Smith, G. M. Hale, G. Arbanas, R. Arcilla, C. R. Bates, B. Beck, B. Becker, F. Brown, R. J. Casperson, J. Conlin, D. E. Cullen, M.-A. Descalle, R. Firestone, T. Gaines, K. H. Guber, A. I. Hawari, J. Holmes, T. D. Johnson, T. Kawano, B. C. Kiedrowski, A. J. Koning, S. Kopecky, L. Leal, J. P. Lestone, C. Lubitz, J. I. Márquez Damián, C. M. Mattoon, E. A. Mccutchan, S. Mughabghab, P. Navratil, D. Neudecker, G. P. A. Nobre, G. Noguere, M. Paris, M. T. Pigni, A. J. Plompen, B. Pritychenko, V. G. Pronyaev, D. Roubtsov, D. Rochman, P. Romano, P. Schillebeeckx, I. Stetcu, P. Talou, I. Thompson, S. Van Der Marck, L. Welser-Sherrill, D. Wiarda, M. White, J. L. Wormald, R. Q. Wright, M. Zerkle, G. Zerovnik, and Y. Zhu, “ENDF/B-VIII.0: The 8 th Major Release of the Nuclear Reaction Data Library with CIELO-project Cross Sections, New Standards and Thermal Scattering Data,” *Nuclear Data Sheets*, vol. 148, pp. 1–142, 2018.
- [14] J.-C. Sublet, D. Cullen, and R. MacFarlane, “How accurately can we calculate fast neutrons slowing down in water?,” *Nuclear Technology*, vol. 168, no. 2, pp. 293–297, 2009.
- [15] J. Goorley *et al.*, “Initial MCNP6 Release Overview - MCNP6 version 1.0,” Tech. Rep. LA-UR-13-22934, Los Alamos National Laboratory, 2013.
- [16] P. K. Romano, N. E. Horelik, B. R. Herman, A. G. Nelson, B. Forget, and K. Smith, “OpenMC: A state-of-the-art Monte Carlo code for research and development,” *Annals of Nuclear Energy*, vol. 82, pp. 90–97, aug 2015.
- [17] X. X. Cai and T. Kittelmann, “NCrystal,” <https://doi.org/10.5281/zenodo.853186>.